Journal of Civil Structural Health Monitoring
https://doi.org/10.1007/s13349-023-00701-9

ORIGINAL PAPER

Validation of an FE model updating procedure for damage assessment using a modular laboratory experiment with a reversible damage mechanism

Marlene Wolniak[1] · Benedikt Hofmeister[1] · Clemens Jonscher[1] · Matthias Fankhänel[1] · Ansgar Loose[1] · Clemens Hübler[1] · Raimund Rolfes[1]

Received: 12 November 2022 / Accepted: 9 April 2023

Abstract
In this work, the systematic validation of a deterministic finite element (FE) model updating procedure for damage assessment is presented using a self-developed modular laboratory experiment. A fundamental, systematic validation of damage assessment methods is rarely conducted and in many experimental investigations, only one type of defect is introduced at only one position. Often, the damage inserted is irreversible and inspections are only performed visually. Thus, the damage introduced and, with it, the results of the damage assessment method considered are often not entirely analyzed in terms of quantity and quality. To address this shortcoming, a modular steel cantilever beam is designed with nine reversible damage positions and the option to insert different damage scenarios in a controlled manner. The measurement data are made available in open-access form which enables a systematic experimental validation of damage assessment methods. To demonstrate such a systematic validation using the modular laboratory experiment, a deterministic FE model updating procedure previously introduced by the authors is applied and extended. The FE model updating approach uses different parameterized damage distribution functions to update the stiffness properties of the structure considered. The mathematical formulation allows for an updating procedure that is independent of the FE mesh resolution and free of assumptions about the defect location while only needing few design variables. In this work, the FE model updating procedure is based only on eigenfrequency deviations. The results show a precise localization within ± 0.05m of the nine different damage positions and a correct relative quantification of the three different damage scenarios considered. With that, first, it is shown that the deterministic FE model updating procedure presented is suitable for precise damage assessment. Second, this work demonstrates that the opportunity to introduce several reversible damage positions and distinctly defined types and severities of damage into the laboratory experiment presented generally enables the systematic experimental validation of damage assessment methods.

Keywords Experimental validation · FE model updating · Damage assessment · Numerical optimization · Modal analysis

1 Introduction

Monitoring engineering structures has become a vital part of civil engineering [1, 2] and a variety of different methods are applied in structural health monitoring (SHM) [3–6]. The goal of monitoring is the identification of damage, which Worden et al. [7] defined as changes to the material, geometric properties, or both of these. Thus, to identify damage, the changes in the structural properties have to be identified by comparing at least two different states of the structure considered. Rytter [8] determined four categories which describe the level of damage identification: detection, localization, assessment (i.e., quantification) and consequence (i.e., remaining life-time prediction). Evidently, these levels increase in difficulty and each subsequent level requires the results of the previous one. The focus of this contribution is the introduction of a modular laboratory experiment with reversible damage mechanisms for the validation of SHM procedures addressing the third level—damage assessment, including the detection, localization and quantification of damage.

✉ Marlene Wolniak
m.wolniak@isd.uni-hannover.de

[1] Institute of Structural Analysis, Leibniz University Hannover / ForWind, Appelstr. 9A, 30167 Hannover, Germany

Published online: 09 May 2023

To examine and validate SHM methods, numerous experimental studies and real-life testing have been conducted over the years. Doebling et al. [9] gave a comprehensive overview of applications of damage identification methods organized according to the type of structure. Examining the various experimental studies, it is noticeable that a great number of the implemented damage scenarios induce material degradation by the application of static loads (cf. e.g., [10, 11]) or by the introduction of saw cuts or kerfs (cf. e.g., [12–14]) into the structure under consideration. These damage mechanisms are irreversible in nature. Hence, usually only one fixed geometric damage location is analyzed in most experiments. However, the damage can be gradually increased in severity, so that different damaged states can be realized at the otherwise predetermined location(s). Regarding the inspection and thus the quantifiability of these common damage scenarios, a kerf can be sawn and measured precisely, whereas the progress of fatigue or creep damage due to loading is difficult to assess. Often, the inspections are only performed visually and the results obtained by the various SHM methods are typically only evaluated regarding the location of the defect inserted, and not its size or shape. The analysis of SHM applications to real-life structures in operation (cf., e.g., [1, 15, 16]) is limited, because there is normally no deliberate, precise defect insertion allowed. If damage is present in a particular structure, it is difficult to inspect thoroughly enough to determine the size and shape of the defects. Again, the results are typically only evaluated in terms of damage localization. Additionally, it is not always given that measurement data from operating structures are available in states before and after the damage event occurred, or there is no clear distinction between these states possible because the damage has occurred gradually.

In conclusion, although SHM methods have been validated in various experimental studies and real-life testing on operating structures, many of these application examples do not provide the opportunity for a thorough analysis and evaluation of the SHM methods considered. Especially in terms of the third level of damage identification, including damage detection, localization and quantification, comprehensive studies are still missing. With regard to the comparability of different SHM methods, another impairment of many of the publications examined is that they do not make the data from their application examples available. Thus, only the described results of the particular SHM method considered are published, leaving no opportunity for a fair comparison of different methods.

Of course, some benchmark problems with open-access raw data in the area of SHM already exist, which provide data for the comparison and analysis of different SHM methods. Prominent laboratory benchmark problems are the three-story building at the Los Alamos National Laboratory (LANL) [17, 18] or the four-story steel frame at the University of British Columbia (UBC) [19, 20]. Widely used benchmark problems involving full-scale engineering structures under environmental and operational conditions (EOCs) are the Z24 bridge in Switzerland [21, 22], the rotor blade of the Vestas V27 wind turbine at the Technical University of Denmark [23–25] and the recently introduced lattice mast structure LUMO at the Leibniz University Hanover [26, 27]. However, these benchmark problems represent rather complicated application examples and are not always suitable when a basic, systematic validation of different SHM methods is sought to be performed.

All in all, the available benchmark problems provide the possibility for a validation and a comparison of different SHM methods. However, they are characterized by rather difficult boundary conditions that complicate a basic validation of different damage assessment methods. This leads to the focus of this contribution, which is the presentation of a modular laboratory steel cantilever beam designed to facilitate a fundamental, systematic experimental validation of damage assessment methods in an entirely controlled setup. The modular experiment is conceptualized with several reversible damage positions and the option to insert different, accurately defined damage scenarios. The motivation for the design of the steel cantilever beam presented was to create a rather simple experiment, in which the structural behavior is entirely comprehensible and different SHM methods can be evaluated and compared at a fundamental level. In addition to the detailed description of the proposed experimental setup, the measurement data are made available in open-access form (see Data Availability Statement) to ensure the opportunity for comparison. To demonstrate the application of the laboratory structure presented, an example systematic experimental validation of an FE model updating procedure addressing the third level of damage identification is outlined. Thereby, a detailed motivation and description of the FE model updating scheme utilized is presented.

This paper consists of six sections. Section 2 gives a detailed description of the experimental setup and the derived FE model used for the model updating procedure. Following this, the modal analysis technique utilized and an analysis of the modal data extracted from the measurements is described in Sect. 3. In addition, a comparison of the dynamic properties of the initial FE model against the extracted modal data from the measurements is highlighted. FE model updating is further introduced in Sect. 4 and the herein considered deterministic FE model updating procedure and the optimization scheme utilized are described in detail. The results are displayed, analyzed and discussed in Sect. 5. Finally, Sect. 6 gives a summary and an outlook.

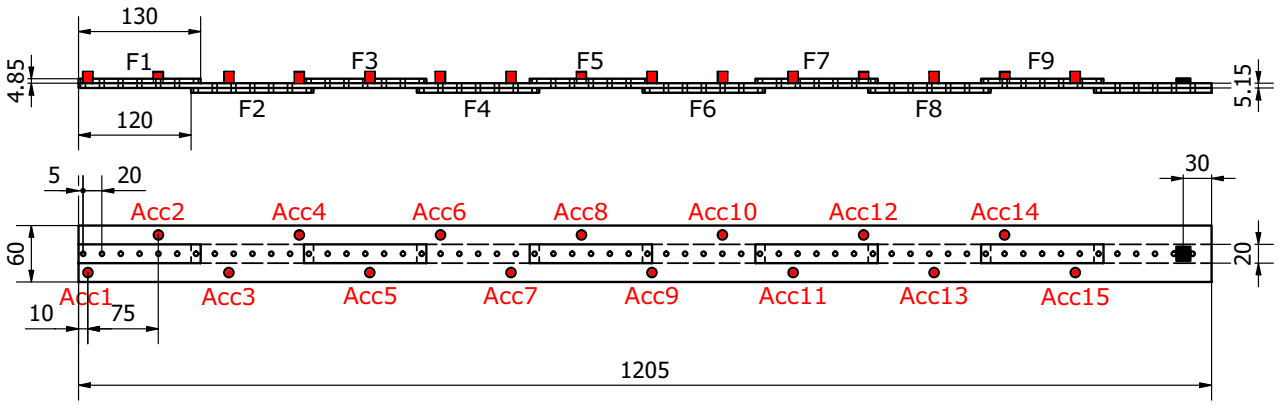

Fig. 1 Schematic overview of the steel cantilever beam. Measures given in mm

Fig. 2 Photograph of the steel cantilever beam

2 Experimental setup

The steel cantilever beam considered is a modular setup of a central beam structure with nine screwed-on fishplates. The fishplates are used to implement a variable, reversible damage mechanism. A schematic overview and a photograph of the modular beam structure are given in Figs. 1 and 2.

The central beam and the screw-on fishplates are fabricated from rectangular stainless-steel bar stock. As depicted in Fig. 1 and visible in Fig. 2, the fishplates are screwed on in alternating positions above and below the central beam structure with an overlap of 10mm. The M5 screws utilized have a uniform separation of 20mm, yielding a total of sixty screws to connect the fishplates to the center line of the central beam. Thus, each fishplate is held in place by seven screws, whereby the overlapping fishplates share one screw at each respective end. To ensure a repeatable fishplate connection stiffness, the screws are tightened with a consistent assembly torque of 5Nm. The fishplates and screw connections are dimensioned to yield contact pressure sufficient to suppress shear movement between the central beam structure and the fishplates by friction. The dimensions of the central beam and the fishplates are listed in Table 1. In addition, a close-up of the tip of the steel cantilever beam is shown in Fig. 3, where the accelerometers, wiring and M5 screws are visible.

The central beam with nine undamaged screw-on fishplates represents the reference state of the considered experiment. The reversible damage mechanism is activated by swapping the intact fishplates with damaged fishplate specimens (see Sect. 2.2 for photographs of the damaged

Table 1 Dimensions of the central beam structure and the screwed-on fishplates

Dimension	Value in mm
Central beam	
Length	1205
Width	60
Thickness	5.15
Fishplates	
Length	130
Width	20
Thickness	4.85

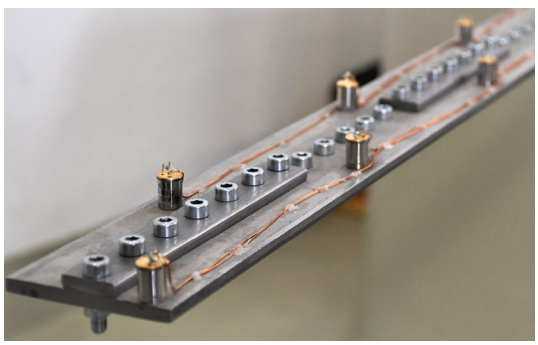

Fig. 3 Close-up of the tip of the steel cantilever beam

fishplate specimens). Since the fishplates are fixed using screws, the mechanism can be activated and deactivated without causing permanent alterations to the structure or the fishplates. As a result, the particular experimental setup with a reversible damage mechanism and different variable damage positions allows for the consideration of a variety of damage scenarios.

2.1 Sensors, measurement system and type of excitation

As the experimental structure is relatively small and light, the sensors are chosen accordingly. A total of fifteen miniature IEPE accelerometers with a dynamic range of $\pm 500 \frac{\mathrm{m}}{s^2}$ are connected to the central beam structure. The sensors weigh only 5g each and are attached along the steel beam with a uniform separation of 75mm using integrated M3 screw connectors. The placement alternates between the right and left side of the beam, as indicated in Fig. 1. This way, also torsional mode shapes can be identified. The accelerometers are connected to the measurement system using enameled copper wires, leaving from the sensors as demonstrated in the close-up view shown in Fig. 3. A terminal block next to the fixed end of the beam is used to connect the enameled copper wires to the measurement lines. The sensors are powered using IEPE current supplies, which are connected to a 24-bit measurement system. Thereby, the use of IEPE sensors ensures rejection of grid hum and a high signal-to-noise ratio [28]. The sampling frequency of the measurement system was set to 1200Hz.

The steel cantilever beam is excited using a proprietary, contact-free electromagnetic shaker placed at the root of the beam (black square in Fig. 1). All measurements were conducted with broadband white-noise excitation up to 250Hz using a signal-generating computer and a digital-to-analog converter connected to a power amplifier. Utilizing broadband white noise ensures the excitation of all eigenmodes in the chosen frequency range.

2.2 Damage scenarios and experimental procedure

For the representation of realistic damage scenarios, structural damage is assumed to manifest itself as stiffness deviations in a certain geometric area of a structure. In the laboratory experiment conducted, damage is introduced by sawing cuts into a fishplate specimen. This locally weakens the cross section of the fishplate. In this work, three different damage scenarios of increasing severity are considered.

One very small, local damage is introduced, subsequently referred to as 'discrete' damage, where the fishplate is sawed into at only one position. The other two fishplates are more severely damaged with saw cuts at six positions equally distributed along the length of the fishplates. Thereby, the length of the saw cuts vary: the saw cut lengths of one fishplate extend from very short cuts at both ends to long cuts in the center. Based on this distribution, this damage scenario is subsequently called 'Gaussian distributed'. The saw cuts of the third damage scenario are of equal length, hence, this damage scenario is referred to as 'uniformly distributed' damage. Due to the relatively long saw cuts, the third damage scenario represents the most severe damage. Figure 4 shows photographs of the three damaged fishplates. Outlines of the total saw cut length(s) are added to further clarify the three different damage scenarios that are to be assessed later on.

The damaged fishplates are designed to have the same weight of 91g as the undamaged fishplates. Since each saw cut has a width of approximately 1mm, some material is removed. To compensate for this, the damaged fishplates are fractions of a millimeter wider than the undamaged ones. This is necessary to guarantee that the changes introduced in the structural dynamic behavior are only due to stiffness variations and not due to mass differences.

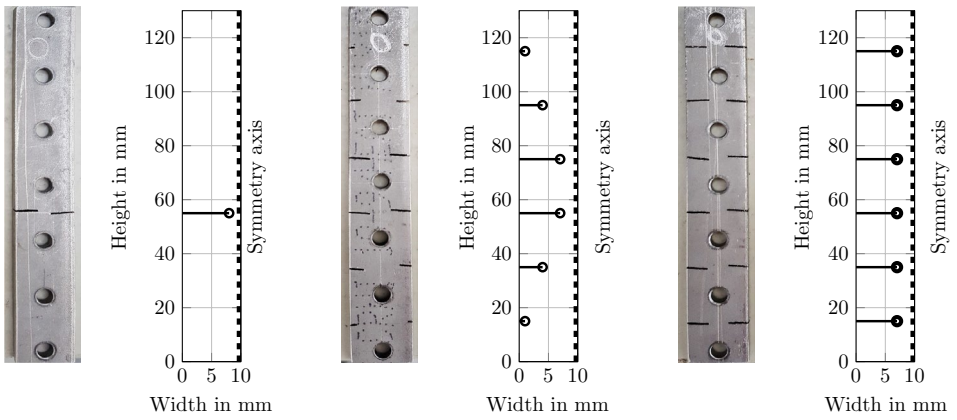

(a) Discrete. (b) Gaussian distributed. (c) Uniformly distributed.

Fig. 4 Photographs of the three differently damaged fishplates and respective diagrams of the saw cut lengths

The experimental procedure comprises three measurement series - one series for each damage scenario (i.e., discrete, Gaussian and uniformally distributed). Each measurement series involves screwing the respective damaged fishplate specimen onto all nine fishplate positions in sequence. In addition, before the measurement of each damaged state of the cantilever beam, the reference state is restored and a measurement of this intact state is conducted. Thus, every measurement series consists of $9 \cdot 2 = 18$ measurements, with each measurement comprising 1 h of data. Table 2 gives an overview of the configuration of the experiments.

For the three measurement series conducted with 18 measurements of 1 h each, this results in a total of 54 h of measurement data. Hence, the experiment was conducted over several weeks, resulting in small changes in the environmental conditions at the experimental site over this time period. Although the experiment was performed in a laboratory, temperature changes and environmental influences like other machinery operating in the laboratory or even small events like people passing the experiment, thus causing vibrations in the laboratory floor, have an effect on the measurements. Additionally, several scientists were involved in the execution and recording of the measurements, resulting in slight differences in the screw-on mounting of the fishplates or the adjustment of the shaker excitation. However, the measurement setup, the setup of the recording measurement system and the method of extraction of the modal data remained identical throughout the whole experiment.

In summary, as is the case for all practical experiments to a greater or lesser degree, there were some influences which affected the measurements that could not be excluded, even though great attention was given to achieving the same conditions for all measurements in all three measurement series. Nevertheless, these influences only caused marginal changes and uncertainties in the measurement and, as a result, in the extracted modal data.

The measurement data used in this work including a comprehensive documentation are uploaded to a public data repository of the Leibniz University Hanover and can be reached under the following link: https://doi.org/10.25835/123gy6gm.

Table 2 Experimental procedure and measurement times

Measurement series	Scenario	Fishplate position			
		1	2	···	9
1	Reference state	1 h	1 h		1 h
	Discrete damage	1 h	1 h		1 h
2	Reference state	1 h	1 h		1 h
	Gaussian distributed damage	1 h	1 h		1 h
3	Reference state	1 h	1 h		1 h
	Uniformly distributed damage	1 h	1 h		1 h

2.3 Finite element model

The aim of the FE model updating procedure considered in this work is damage localization and quantification along the length of the steel cantilever beam. To fulfill this aim, a beam model is chosen as a representation of the steel cantilever beam, as it is sufficient for the task and computationally inexpensive. The latter is important since the FE model updating procedure represents an optimization process, in which the computational costs of multiple evaluations of the underlying numerical model become an issue. With this rather small FE model incorporating few degrees of freedom, the modal analysis step takes only seconds. Thus, extensive numerical studies are made possible.

The simulations are conducted using the FE analysis software Abaqus. For the beam model, two-node linear beam elements (B31) based on Timoshenko beam theory [29] are chosen. Thereby, the length of the finite elements is chosen to be 1mm, corresponding to the saw cut width. The varying sectional properties along the beam structure are assigned to the beam elements using general cross-sectional parameters. Three sections are defined for the fishplates positioned above and below the central beam and where two fishplates overlap (cf. Fig. 1). The sectional properties assigned are listed in Table 3. The material properties of stainless steel are utilized, and the omitted mass due to the screw holes and the additional mass of the sixty screws connecting the fishplates to the central beam are taken into account by adjusting the density of the standard material ($7900\mathrm{kg/m^3}$). Given that the screw holes have an average diameter of 5mm and the average mass of a screw and a nut is 5.1g, the density is increased to a value of $8500\mathrm{kg/m^3}$. The weight of the enameled copper wiring is neglected as this is an insignificantly low weight relative to the bulk of the steel cantilever beam.

Table 3 Sectional properties assigned to the beam elements of the FE model

Section	Description of fishplate position	Area in $\mathrm{mm^2}$	I_{11} in $\mathrm{N/mm^2}$	I_{22} in $\mathrm{N/mm^2}$	J in $\mathrm{N/mm^2}$	Offset center line in mm
1	Above central beam	406	2719	959	5504	1.2
2	Below central beam	406	2719	959	5504	−1.2
3	Overlap	503	5913	992	9526	0

The miniature accelerometers have a mass of 5g each and are simulated as point masses at the corresponding locations along the beam (cf. Fig. 1). The offset of the sensor positions is taken into account by placing additional nodes ± 20mm orthogonally from the center line of the beam, alternating to the left and right, and assigning the point masses to these offset nodes. A kinematic constraint couples the offset nodes to the corresponding nodes of the model. At the root of the steel cantilever beam, all degrees of freedom are set to zero, representing the fixed support. Figure 5 shows the FE model as displayed in the FE analysis software Abaqus with rendered beam profiles and marked sensor positions.

The beam model represents the reference model of the intact steel cantilever beam and is used as the basis for the following FE model updating procedure.

3 Modal analysis

To ensure high-quality modal data as an input for the FE model updating procedure, an advanced identification method is used for the extraction of modal data from the measurements.

3.1 Identification method

The identification method chosen is based on the frequency domain decomposition (FDD) [30]. A singular value decomposition is performed on the power spectral density (PSD) matrix G_{yy} of the structural responses

$$\mathbf{G}_{yy}(f_k) = \mathbf{U}_k \mathbf{S}_k \mathbf{U}_k^H, \tag{1}$$

where f_k is the frequency, $\mathbf{U}_k$ is a unitary matrix of the singular vectors $\mathbf{u}_{ki}$ and $\mathbf{S}_k$ is a diagonal matrix of the singular values s_{ki}. In the case of well-separated modes and white-noise excitation, which are prerequisites of this identification method, only one mode dominates in the vicinity of the natural frequency f_0. As a consequence, the largest singular value dominates close to an eigenfrequency. Peak picking is used to determine the natural frequency and the eigenmode is identified from the corresponding singular vector. The singular value curve in the vicinity of the mode corresponds to the curve of a PSD of a single-degree-of-freedom (SDOF) oscillator [31]. Therefore, a more accurate identification of the natural frequency is achieved by fitting the theoretical PSD h of an SDOF to the measured singular value spectrum. For acceleration signals, the PSD is

$$h(f_0, \zeta, S, e, f_k) = \frac{(2\pi f_k)^4 S^2}{(4\zeta^2 - 2)\eta_k^2 + \eta_k^4 + 1} + e, \quad \eta_k = \frac{f_k}{f_0}, \tag{2}$$

where ζ is the damping ratio, S is the modal force and e denotes the model error. The model error and the modal force are assumed to be constant across the frequency range considered. The model error represents the measurement noise and signal components which do not match the SDOF spectrum. The identification of the four parameters is achieved using numerical optimization. The resulting least-squares problem is

$$\min \left(\sum_{k=k_\mathrm{l}}^{k_\mathrm{u}} \left(h(f_0, \zeta, S, e, f_k)^2 - s_{k1}^2 \right) \right), \tag{3}$$

where k_l and k_u are the indices of the lower and upper frequency limits of the range under consideration.

In addition to the prerequisites already mentioned, modal damping is assumed and, naturally, the settings of the sampling rate have to fit the frequency range of interest. Therefore, it is referred to Brincker and Ventura [32], where it is recommended that

$$f_s > 2.4 f_{\max}. \tag{4}$$

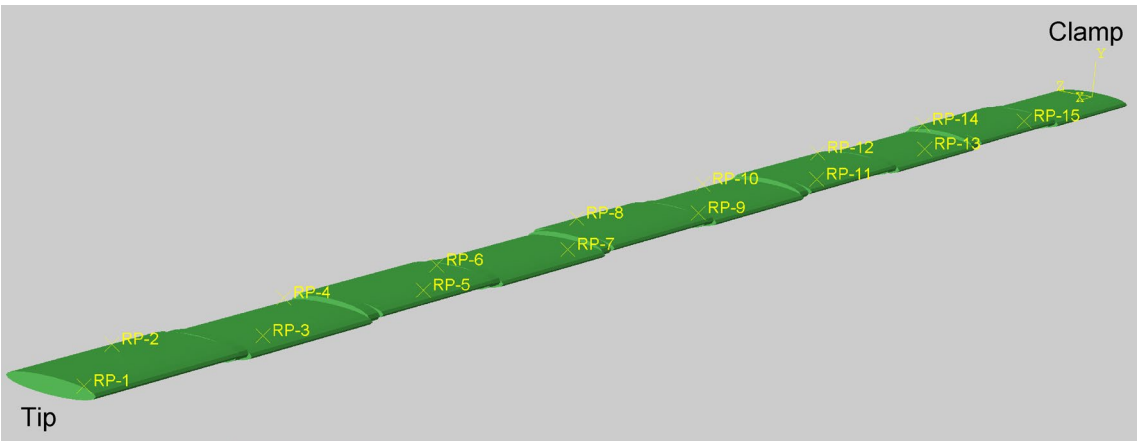

Fig. 5 FE model of the steel cantilever beam with rendered beam profiles and sensor locations marked as reference points

Thereby, f_s is the sampling frequency and $f_{\max}$ is the highest frequency of interest. The choice of the measurement time determines the accuracy desired, whereby Brincker and Ventura [32] give indications regarding the required minimum measurement time T depending on the lowest frequency of interest $f_{\min}$ and the damping ratio ζ

$$T > \frac{10}{\zeta f_{\min}}. \tag{5}$$

3.2 Extracted modal data

Before a detailed overview of the extracted modal properties in both the reference state and the different damaged states is given in the following two subsections, an insight into the identification settings used for the extraction of the modal data is presented. As the attached accelerometers measure only in the vertical direction, horizontal mode shapes are not recorded properly. Occurring torsional modes can be identified due to the alternating placement of the accelerometers (cf. Sect. 2). Nevertheless, horizontal and torsional modes are not sufficiently excited for a distinct identification using the FDD, because the excitation applied to the steel cantilever beam exclusively operates in the vertical direction. Thus, only the modal properties corresponding to pure vertical bending modes are included in the subsequent FE model updating procedure and all other modes are neglected in this work. The alternating sensor positions were chosen anticipatory as subsequent applications might include a differing excitation.

Table 4 lists the frequency ranges applied for the first four extracted eigenfrequencies related to pure vertical bending mode shapes and in Table 5 other identification settings regarding, e.g., the sampling rate, measurement time and window length are given. As the measurement time is chosen differently in the subsequent evaluations, it is listed as a value t. Thereby, the setup of the laboratory experiment and the identification settings fulfill the prerequisites necessary for the identification of the modal properties using the FDD method. Broadband white noise is used as excitation, the modes are well-separated and the chosen sampling rate of 1200Hz covers the frequency range of interest well with regard to Eq. 4.

Table 4 Frequency range used for the extraction of the modal data

Eigenfrequency no	f_{l} in Hz	f_{u} in Hz
1	3	5
2	22	25.5
3	60	80
4	195	235

Table 5 Identification settings used for the extraction of the modal data

Setting	Assignment
Sampling rate	1200 Hz
Measurement time	t in s
Window	Hanning
Window length	1200 Hz $\cdot t$
Zero padding	0
Overlapping data points	0

3.2.1 Reference state and comparison to the finite element model

According to the design of the experiments outlined in Table 2, the reference state of the cantilever beam was reconstituted and measured for a total of $9 \cdot 3 = 27$ times, resulting in 27 h of measurement data. As already mentioned in Sect. 2, some environmental conditions and personal influences affected the measurement data. This is why the extracted modal data from the 27 h of measurement in the reference state show small variance, which is presented and analyzed in the following.

Table 6 gives an overview of the statistical data of the four eigenfrequencies identified from all 1 h-measurements in the reference state (i.e., $t = 3600$ s). Furthermore, the corresponding eigenfrequencies calculated with the previously introduced FE model are listed together with their percentage deviation (Δf) from the median value of the respective eigenfrequency extracted from the measurements. Thereby, the corresponding eigenmodes are selected by employing the well-known modal assurance criterion (MAC) defined by Allemang [33]. The MAC determines the degree of similarity between two mode shape vectors, returning a value of one if the mode shapes compared are linearly dependent, and a value of zero if they are linearly independent. Naturally, the allocation of the simulated mode shapes to the measured ones is decided with respect to the highest MAC value. Figure 6 visualizes the MAC values of the vertical mode shape deflection at the fifteen sensor positions shared by the four measured and the first ten simulated mode shapes in the reference state.

As is evident from Fig. 6, the matching of the simulated mode shapes to those extracted from the measurements based on the MAC value alone gives a conclusive result for the first, third and fourth measured mode shapes. The second measured mode shape shows a high correlation to both the second and third simulated mode shapes. Here, a distinct selection can be reached by considering the deflection

Table 6 Quartile values of the four extracted eigenfrequencies from all 1 h-measurements in the reference state and a comparison to the corresponding modal properties calculated with the FE model

Eigen-	Measurement			FE model	Comparison	
frequency	first quartile	Median	Third quartile		Δf	MAC
no	in Hz	in Hz	in Hz	in Hz	in %	–
1	3.931	3.934	3.940	3.90	− 0.86	0.9989
2	24.478	24.503	24.516	24.44	− 0.26	0.9984
3	68.251	68.353	68.406	68.43	0.11	0.9965
4	218.644	218.851	219.127	221.39	1.16	0.9848

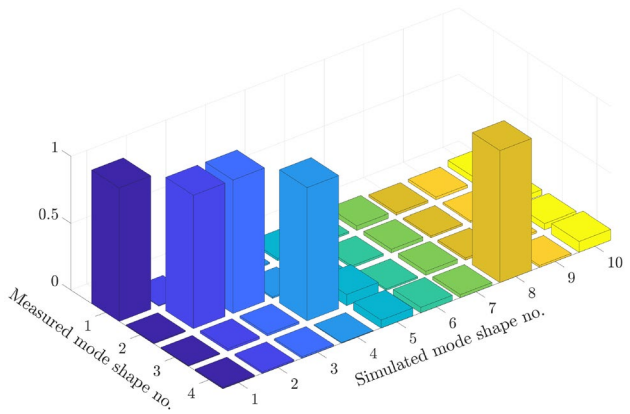

Fig. 6 MAC values of the vertical mode shape deflection at the fifteen sensor positions shared by the measured and simulated mode shapes in the reference state

direction of the simulated modes. As the second simulated mode shape has its main deflection amplitude in the horizontal direction, this horizontal bending mode can be eliminated, despite showing a high MAC value with respect to the second measured shape. The actual deflection shapes of the first four bending modes extracted from the measurements in the reference state are shown in Fig. 7. In conjunction with Table 6, Fig. 7 depicts the 1 h-median values of the normalized vertical deflection amplitude at the fifteen sensor positions. Furthermore, the values of the normalized vertical deflection amplitude at the fifteen (simulated) sensor positions of the corresponding simulated mode shapes are added. To support the visualization, the discrete values at the sensor positions are connected by linear interpolation.

3.2.2 Damaged states

The damaged states are obtained by swapping the intact fishplates with damaged fishplate specimens in sequence. Thus, a total of 27 different damaged states were measured (cf. Table 2). Thereby, each geometric position and each damage scenario influences the modal properties of the steel cantilever beam in a different way.

To provide an overview of the effect of the different damaged states, the alteration of the first and second eigenfrequency is considered in more detail. For an increase of the statistical evidence, all 1 h-measurements of the different damaged states are divided into six 10-min data sets. Thereby, a measurement time of ten minutes with the lowest frequency of interest at approximately 3.9Hz clearly exceeds the required minimum measurement time (cf. Equation 5) for the application of the FDD method. Figures 8 and 9 show the boxplots of the first and second eigenfrequency extracted from the discrete and the uniformly distributed damage state, using the 10-min data sets. To render the variations of the damaged states with respect to the reference state, a solid line is added to indicate the median value and two dashed lines are added to indicate the first and third quartile values of the corresponding eigenfrequencies extracted in the reference state (cf. Table 6).

First of all, an observation of the eigenfrequency deviations in Figs. 8 and 9 clearly reveals a stiffness reduction of the beam caused by a screw-on of the damaged fishplate specimens: The eigenfrequencies extracted from the damage scenarios are primarily lower than the median value of the corresponding eigenfrequencies extracted in the reference state.

As the damage scenarios considered range from small to more severe stiffness alterations (cf. Fig. 4), their influence on the modal properties of the steel cantilever beam differ, respectively. In the following, the intensity of the influence of each damage scenario is examined using the example of the alteration of the first eigenfrequency and the damaged fishplate position 9. Table 7 lists the median value of the first eigenfrequency extracted from the 10-min data sets of each damage scenario of fishplate position 9. In addition, the percentage deviation with respect to the corresponding median value of 3.934Hz is listed, calculated using all 27 1-h measurements in the reference state (cf. Table 6).

Table 7 clearly demonstrates that the increasing severity of the three damage scenarios is reflected in the intensity of the eigenfrequency deviation. Whereas the deviation caused by the Gaussian distributed damage only slightly increases with regard to the deviation caused by the discrete damage,

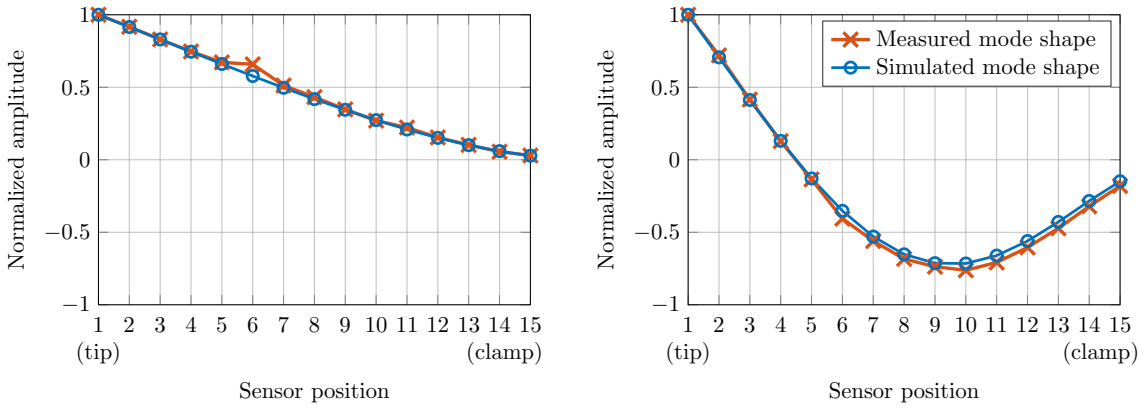

(a) Measured mode shape no. 1 and simulated mode shape no. 1.

(b) Measured mode shape no. 2 and simulated mode shape no. 3.

(c) Measured mode shape no. 3 and simulated mode shape no. 4.

(d) Measured mode shape no. 4 and simulated mode shape no. 8.

Fig. 7 Comparison of the normalized vertical deflection amplitude of the first four bending modes extracted from all measurements in the reference state with the selected simulation results at the fifteen sensor positions

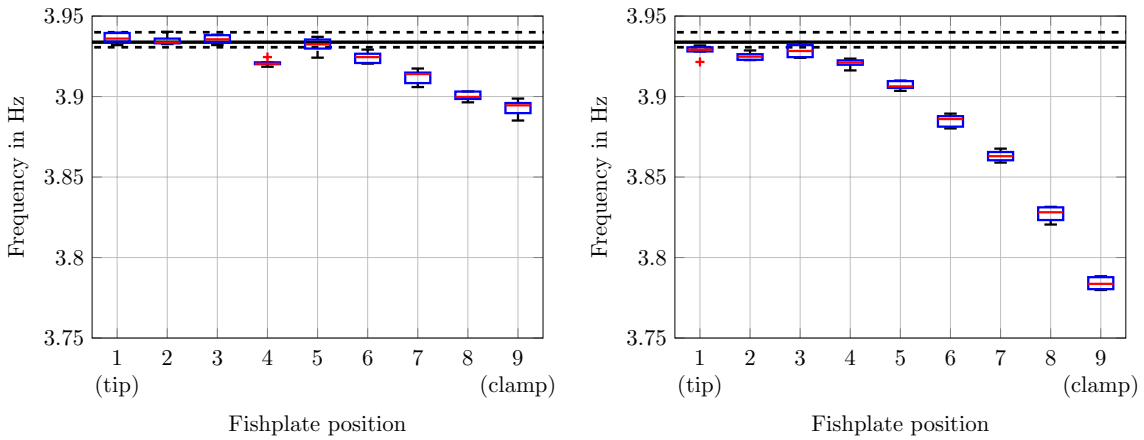

(a) Discrete.

(b) Uniformly distributed.

Fig. 8 Boxplots of the first eigenfrequency extracted from the discrete and the uniformly distributed damage scenario. The solid line indicates the median value and the dashed lines indicate the first and third quartile values of the corresponding eigenfrequency in the reference state

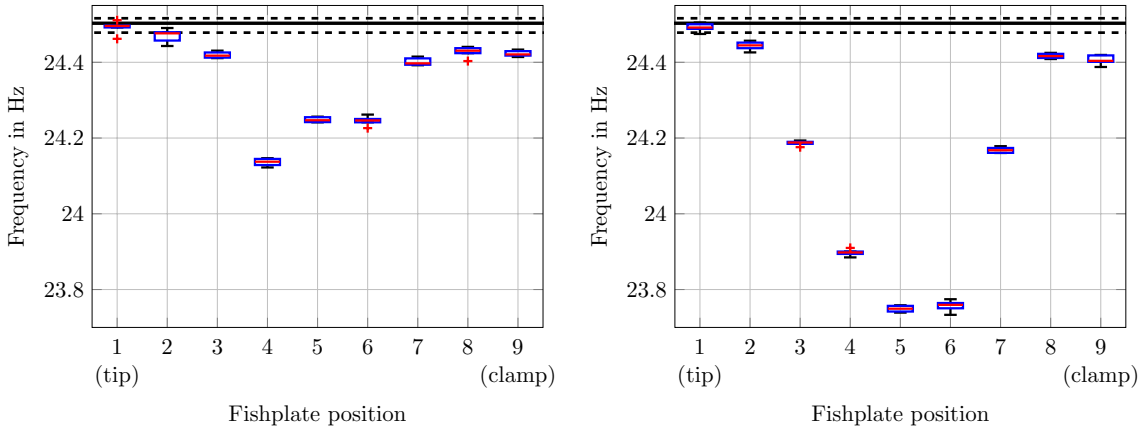

(a) Discrete. (b) Uniformly distributed.

Fig. 9 Boxplots of the second eigenfrequency extracted from the discrete and the uniformly distributed damage scenario. The solid line indicates the median value and the dashed lines indicate the first and third quartile values of the corresponding eigenfrequency in the reference state

the uniformly distributed damage yields a deviation more than twice as large as the other two damage scenarios.

In addition to the severity of the damage, its geometric position along the length of the beam plays an important role regarding the influence on the modal properties. Thereby, the influence of each geometric position additionally varies with regard to the eigenfrequency considered. An observation of Figs. 8 and 9 reveals that, for instance, a damage position near the bearing (i.e., fishplate position 9) greatly affects the first eigenfrequency but has no noticeable effect on the second eigenfrequency. This is explained by the deflection shape: With the corresponding measured mode shapes in mind (cf. Fig. 7), it is evident that a high eigenfrequency deviation occurs at the geometric positions where the corresponding mode shapes show a high curvature. Geometric positions with a low curvature—i.e., the geometric positions of the zero crossings—show a low deviation in the eigenfrequency extracted.

This observation emphasizes the well-known need for the inclusion of several eigenfrequencies in the objective function of the FE model updating procedure for the localization of all damaged fishplate positions along the length of the steel cantilever beam: The geometric position of the damage evidently possesses different effects on the different eigenfrequencies.

Table 7 Median values of the first eigenfrequency extracted from the 10-min data sets of the three damage scenarios of fishplate position 9 and comparison with the respective median value of 3.934 Hz extracted from all measurements in the reference state

Damage scenario	Median in Hz	Δf in %
Discrete	3.895	− 0.99
Gaussian distributed	3.877	− 1.45
Uniformly distributed	3.784	− 3.81

4 Finite element model updating

As part of the vibration-based non-destructive damage assessment methods, the basic assumption of FE model updating is that damage-induced variations in the mechanical properties cause detectable changes in the structural dynamic behavior [34, 35]. Thus, to detect, locate and quantify damage, vibration measurement data are analyzed and damage features are extracted. In a second step, an FE model is updated to match the structural behavior observed. Most often, this is done in terms of stiffness deviations [36]. As hands-on trial and error approaches are time consuming and not feasible for complex engineering structures, the problem is formulated indirectly as an optimization problem [15, 37]. Thereby, the objective function compares the dynamic behavior of the numerical model to a target (i.e., damaged) state and an optimization algorithm is used to find a model to match this target state by modifying stiffness parameters of the respective parameterized FE model. As the excitation forces are not known for output-only measurement setups in civil engineering applications, the measured time domain data are of little use for FE model updating approaches. Thus, the objective function generally comprises the difference of modal parameters or transfer functions, extracted from the measured data using signal processing and modal analysis techniques.

A variety of applications of different FE model updating methods on numerical examples and experimental investigations has been conducted over the last years [3, 34, 35], pointing out and aiming to overcome several difficulties of

model updating. Many issues arise due to two major sources of uncertainty affecting the model updating process.

One source of uncertainty is the measurement data itself, including further processing of the gathered data. Due to the inevitable spatial sparsity and noisiness of the measured data and also due to imperfections in the measurement equipment and setup, measured data is always a source of errors and uncertainty [38]. By careful planning of the measurement system and sensor setup, possible error sources might be discovered and removed. Considering incomplete and noisy measurement data, many attempts are made to generalize or regulate this source of uncertainty [39]. However, the fact remains that measurement uncertainty can merely be minimized, but never be fully eliminated. Even more uncertainty is introduced during the subsequent signal processing and extraction of modal characteristics of the physical structure [36]. Thereby, the outcome depends on the choice and application of the modal analysis technique [40]. This source of uncertainty can be addressed by applying uncertainty quantification. Examples for uncertainty quantification in model updating are probabilisitc Bayesian approaches [41–44] and non-probabilistic fuzzy approaches [45–47]. However, in this work, FE model updating is applied solely in the deterministic sense. Uncertainties due to measurement noise or further signal processing is sought to be minimized using a low-noise measurement setup (cf. Sect. 2.1) and an advanced identification method for the extraction of modal data (cf. Sect. 3.1).

The second major source of possible uncertainties is the FE model used in the updating procedure. Mottershead et al. [15] classified the sources of modeling uncertainties into reducible and irreducible by model updating. By their definition, reducible sources are erroneous assumptions for model parameters, like material or geometric properties. Thus, the correction of these properties is the aim of every model updating procedure. Irreducible sources are discretization errors and idealization errors made, e.g., in the process of simplifying the mechanical behavior. The requirement derived from these assessments is that numerical models need to be validated prior to their use for updating, so that at the end of the model updating process all three kinds of modeling uncertainties are minimized. In this work, this recommendation is adapted by validating the FE model prior to the model updating process. Thereby, the introduced FE model described in Sect. 2.3 was examined and enhanced, e.g., regarding the consideration of the mass increase due to the wiring and sensors. As oftentimes a constant systematic difference between the simulated modal quantities of the initial but validated FE model and the extracted modal quantities of the measurement remains, a formulation of a normalized relative objective function is chosen in this work. This enables the mitigation of inherent constant systematic errors between model and measurement.

Regarding the correction of the model parameters, a variety of different approaches exists [36]. Commonly, design variables are mapped directly to structural properties such as stiffness values of individual finite elements. If the defect location is unknown, this procedure usually entails a large amount of design variables, resulting in an objective value space with many local minima. Thus, many authors aim to keep the amount of design variables as low as possible. A common example is to divide the numerical model into groups of FEs and mapping one design variable per structural property of these formed FE groups [48–50]. Another example is to observe only a geometrically restricted area of the model, whereby, naturally, a prior assumption of the defect location is required [14, 51]. Additionally, if the design variables are not constrained, the updating might result in oscillatory stiffness values which can produce almost the same response as correct values, despite being physically unrealistic [48, 52].

To address this problem, the application of a parameterized damage distribution function was previously introduced by the authors [53, 54] and is utilized and extended in this work. The FE model updating approach proposed using a damage distribution function is independent of the FE mesh resolution and of prior assumptions about the defect location while only needing few design variables. By formulating the mapping of the considered structural properties to the finite elements using a cumulative distribution function, a smooth, realistic distribution is ensured. This forces the model updating process to focus on global structural dynamics instead of over-fitting local deviations. As different damage scenarios like a cut or a stiffness degradation have diverging effects on the stiffness properties of the structure, the method is extended by the possibility to exchange different damage distribution functions. This offers the opportunity to imitate the damage behavior and, with that, the damage scenario as good as possible. In addition, using different damage distribution functions and a relative formulation of the objective function, many of the mentioned issues of common FE model updating procedures are addressed. Thereby, the goal is to obtain a numerically efficient, well-posed optimization problem, which can handle irreducible modeling errors.

Other approaches, that are also motivated by smoothly distributed structural properties and the reduction of the number of design variables, are analyzed and successfully used in [11, 49, 55]. Contrary to the approach proposed by the authors, these methods use linear or quadratic functions to describe a so-called damage function. In addition, FEs are still grouped in these approaches. Schommer et al. [56, 57] modified the approach by Teughels et al. [58] and defined a Gaussian bell curve to describe a damage function. Whereas the basic idea of this approach has similarities to the one proposed in this work, the mathematical formulation and the

implementation of the updating methodology, including the optimization process, differ significantly from each other.

4.1 Design variables

The formulation of the design variables strongly depends on the problem to be solved using model updating. Since the aim of this work is damage localization along the length of the steel cantilever beam and damage quantification, the parameterization should be able to identify the geometric location of the damage and its intensity.

As damage manifests itself as a change in stiffness, the general approach for most FE model updating procedures with the aim of damage assessment is to alter the stiffness properties of the model at hand [36]. This approach is also employed in this work. As no prior knowledge about the defect location is assumed for the procedure proposed, an updating of the stiffness property of all n elements along the length of the numerical model is chosen. This is implemented by adapting the initial Young's modulus E^0 of each finite element with a corresponding scaling factor θ_i

$$E_i^{\theta} = \theta_i \cdot E^0, \quad i \in [1, n]. \tag{6}$$

The stiffness scaling factors θ_i are calculated on the basis of the design variables, which, in turn, parameterize a damage distribution function. Thereby, the modular setup of the presented damage assessment method is demonstrated by the use of two different damage distribution functions, whereby their application to the three different damage scenarios is analyzed. The possibility to use different damage distribution functions allows the best possible replication of the damage scenario and a comparison between the results. In this work, a Gaussian and a continuous uniform damage distribution function are considered exemplary.

Both distribution functions are defined along one control variable—the length of the beam L—and described by the three design variables

$$\boldsymbol{x} = (\mu \;\; \sigma \;\; D)^{\mathrm{T}}. \tag{7}$$

In the design variable vector $\boldsymbol{x}$, μ represents the geometrical position of the distribution function's center point along the length, σ represents the width of the distribution and D represents the intensity of the damage. The particular affiliations of the design variables corresponding to the two different damage distribution functions are depicted in Fig. 10 for the example design variable vector $\boldsymbol{x} = (0.4\text{m} \;\; 0.1\text{m} \;\; 0.025)^{\mathrm{T}}$. Thereby, the definitions of D and μ are similar while the definition of σ varies slightly. Regarding the continuous uniform distribution function, 100% of the realizations correspond to $\pm\sigma$. Regarding the Gaussian distribution function, only 68.27% of the realizations correspond to $\pm\sigma$ and 95.45% correspond to $\pm 2\sigma$. This association represents the definition of a standard Gaussian distribution function.

The damage intensity can be described as

$$D = \frac{1}{L} \int_{\mathrm{L}} 1 - \theta(s_{\mathrm{L}}) \, ds_{\mathrm{L}}, \tag{8}$$

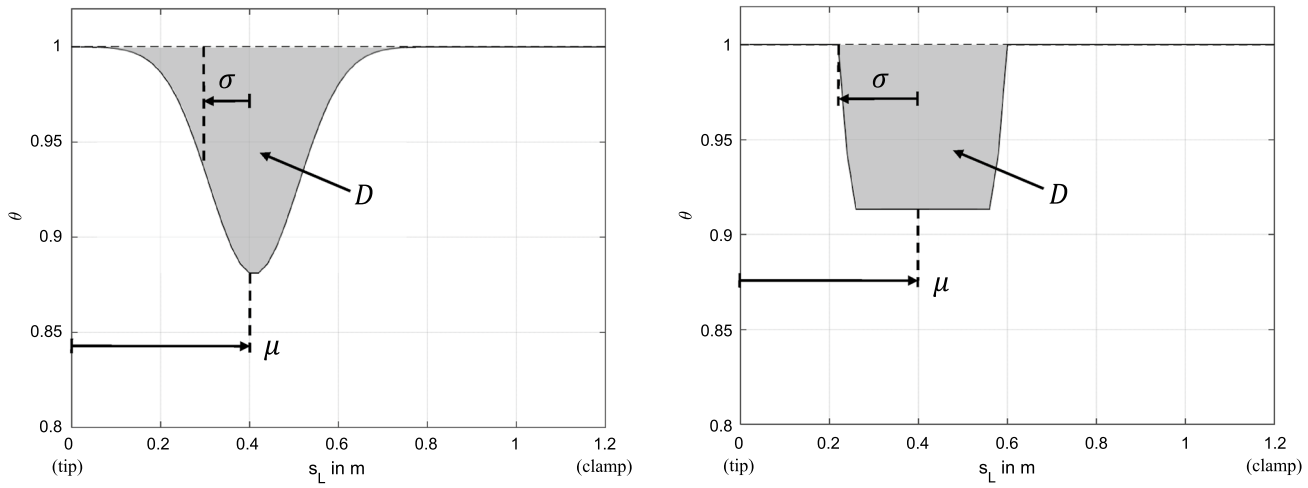

(a) Gaussian.

(b) Continuous uniform.

Fig. 10 Affiliations of the three design variables demonstrated for the example design variable vector $\boldsymbol{x} = (0.4\text{m} \;\; 0.1\text{m} \;\; 0.025)^{\mathrm{T}}$ for the two damage distribution functions considered

where L is the total length of the steel cantilever beam, s_L is the control variable along the beam length and $\theta(s_\mathrm{L})$ is the stiffness scaling factor at position s_L. Relating this to the FE model, a stiffness scaling factor θ_i is assigned to each element. Thus, the discrete damage intensity can be expressed as the sum over the total number of elements along the length

$$D = \frac{1}{L}\sum_{i=1}^{N_\mathrm{L}}(1-\theta_i)(s_{\mathrm{L},i+1} - s_{\mathrm{L},i}). \tag{9}$$

Thereby, the term $s_{\mathrm{L},i+1} - s_{\mathrm{L},i}$ is the actual length of every element. For the calculation of the stiffness scaling factor θ_i for each element, the respective cumulative distribution functions $F\left(s_{\mathrm{L},i}|\mu,\sigma\right)$ of the damage distribution functions considered are truncated to the interval $0 \leq s_{\mathrm{L},i} \leq L$

$$\theta_i = 1 - DL\,\frac{F\left(s_{\mathrm{L},i+1}|\mu,\sigma,0,\mathrm{L}\right) - F\left(s_{\mathrm{L},i}|\mu,\sigma,0,\mathrm{L}\right)}{s_{\mathrm{L},i+1} - s_{\mathrm{L},i}}. \tag{10}$$

Figure 11 shows the distribution of the stiffness scaling factors θ_i calculated for the same example design variable vector and an example FE segmentation along the beam length. Additionally, the respective cumulative distribution functions are displayed with values circled at each element position $s_{\mathrm{L},i}$. It should be clarified that the two damage distribution functions do not represent probability distributions.

In summary, different damage distribution functions can be realized and easily exchanged with the presented parameterization, whereupon the model updating procedure is able to imitate different damage modes. Therefor, only few—in this case three—design variables are necessary. This emphasizes the advantage of the use of a damage distribution function instead of mapping design variables directly to structural properties.

4.2 Objective function

In this work, the FE model updating is based on eigenfrequencies, since these can be obtained experimentally and under operational conditions in high quality. Only $N_\mathrm{freqs} = 4$ eigenfrequencies with a significant amplitude in vertical direction are considered, as described in detail in Sect. 3. To evaluate the difference between the relevant measured (i.e., target) and simulated eigenfrequencies, the root mean square error is utilized

$$\epsilon(\boldsymbol{x}) = \sqrt{\frac{1}{N_\mathrm{freqs}}\sum_{k=1}^{N_\mathrm{freqs}}\left(\frac{f_{\mathrm{SD},k}(\boldsymbol{x}) - f_{\mathrm{SR},k}}{f_{\mathrm{SR},k}} - \frac{f_{\mathrm{MD},k} - f_{\mathrm{MR},k}}{f_{\mathrm{MR},k}}\right)^2}. \tag{11}$$

In this equation, the eigenfrequencies f are denoted with a subscript $(\cdot)_\mathrm{S}$ for simulated and $(\cdot)_\mathrm{M}$ for measured data. In addition, the subscript $(\cdot)_D$ refers to the damaged state, while $(\cdot)_R$ refers to the undamaged reference state. Thereby, the design variable vector $\boldsymbol{x}$ only influences the simulation results of the damaged states, while all other terms of Eq. 11 remain constant during the optimization run. With this relative formulation of the objective function a constant initial error between the simulation and the measurement results in their respective reference states can be taken into account.

As the value range of the stiffness scaling factors is not restricted to positive values by Eq. 10, negative values for θ_i can arise for low values of σ, leading to meaningless FE results. To avoid this issue, all FE models with negative stiffness values are rejected prior to the FE calculation. Since this approach creates a discontinuity in the objective function, a constraint is added to facilitate the optimization process. Therefore, the minimum stiffness scaling factor is used to formulate an inequality constraint which acts to restrict

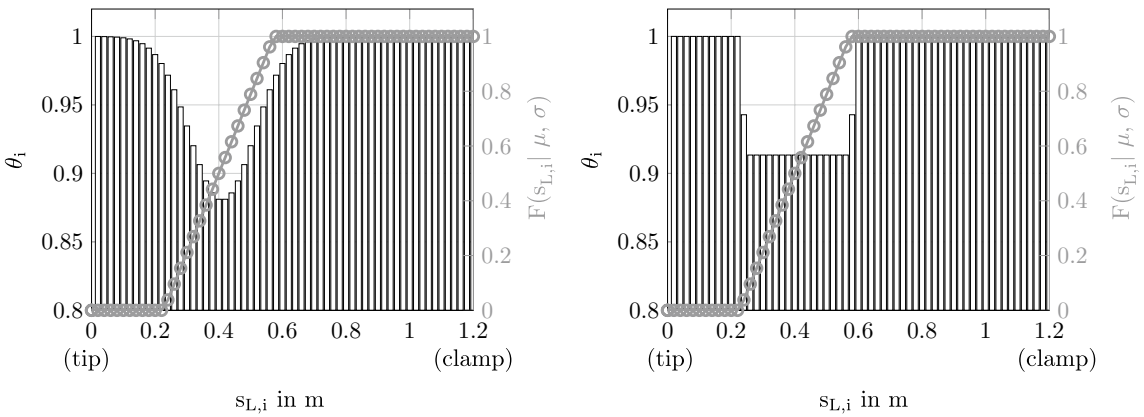

(a) Gaussian. (b) Continuous uniform.

Fig. 11 Distributions of the stiffness scaling factors θ_i and the corresponding cumulative distribution function $F\left(s_{\mathrm{L},i}|\mu,\sigma,0,\mathrm{L}\right)$ with values circled at each element positions $s_{\mathrm{L},i}$ for the example design variable vector $\boldsymbol{x} = (0.4\,\mathrm{m}\ \ 0.1\,\mathrm{m}\ \ 0.025)^\mathrm{T}$

values below 15% of the original stiffness. This leads to the formulation of the bounded and constrained single-objective optimization problem

$$\begin{aligned} &\text{minimise } \epsilon(\boldsymbol{x}) \\ &\text{s.t.} \left[0\text{m} \;\; 0\text{m} \;\; -0.1 \right]^T \leq \boldsymbol{x} \leq \left[1.205\text{m} \;\; 0.2\text{m} \;\; 0.1 \right]^T \\ &\text{s.t.} \min_i \left(\theta_i \right) > 0.15. \end{aligned} \tag{12}$$

The constraint is enforced using the exterior linear penalty method [59].

4.3 Optimization scheme

The in-house object-oriented optimization framework EngiO [60] is utilized for the numerical optimization. For the optimization procedure, the deterministic Global Pattern Search algorithm [61] is chosen, as this algorithm was previously tested and performed well on various similar FE model updating procedures [53, 54]. The parameter T, defining the number of points tracked in the design variable space, is set to 20. The connection between the optimization framework—written in Matlab programming syntax—and the FE calculations using Abaqus is also implemented using Matlab. Thereby, the input file of the FE model is adapted with the new design variable vector of each optimization step as described in Sect. 4.1. Next, the FE calculation is started and afterwards the result file containing the simulated eigenfrequencies is evaluated and the objective function is calculated. Based on the result, a new design variable vector is provided by the optimization algorithm and the procedure is repeated. To ensure comparability of the different optimization runs, the maximum number of the objective function evaluations is set to 1500 for all data sets. Initially, this number was set based on experience from prior applications with only few design variables and a single-objective optimization problem. The convergence behavior of the first optimization runs subsequently confirmed that the chosen number of maximum evaluations is sufficient.

5 Results

As introduced in Sect. 3, the 1-h measurements are divided into six 10min-data sets each. This division is also employed for the application of the FE model updating procedure. For each of the 27 damaged states (i.e., 3 damage scenarios times 9 fishplate positions), six optimization runs are conducted. Therefore, the eigenfrequencies used as input for the calculation of the objective function (cf. $f_{\mathrm{MD},k}$ in Eq. 11) are the six 10-min median values extracted from the considered 1-h measurements. This results in $27 \cdot 6$ optimization results per damage distribution function applied. The eigenfrequencies of the reference state ($f_{\mathrm{MR},k}$) used in Eq. 11 are the respective median values of all 1-h measurements in the reference state listed in Table 6.

Before the optimal results are shown, two different example convergence behaviors are given using the Gaussian distributed damage scenario of fishplate positions 1 (tip) and 9 (clamp). For these examples, the Gaussian damage distribution function is employed. Figure 12 depicts the convergence behavior of the corresponding best objective function values and Figs. 13 and 14 show the convergence

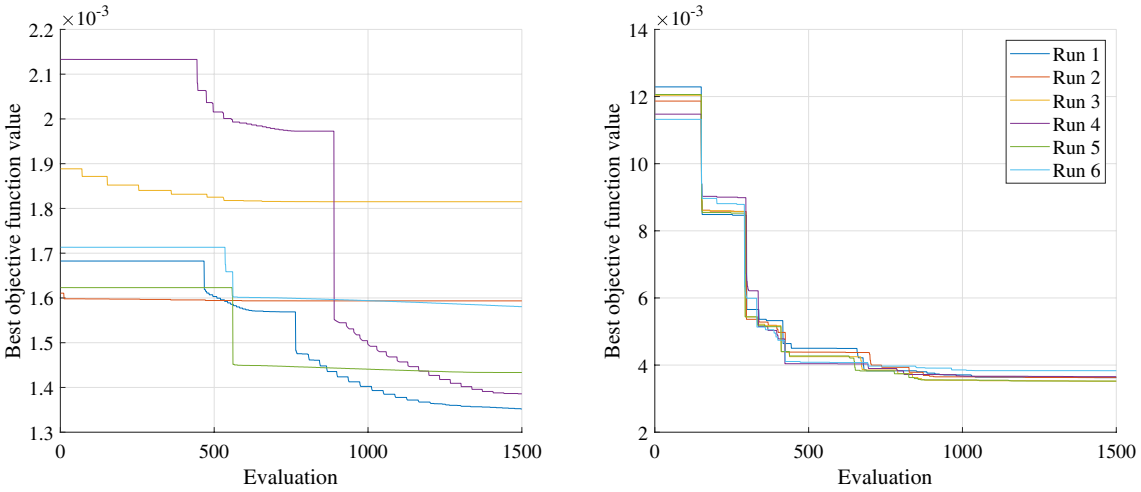

(a) Fishplate position 1 (tip). (b) Fishplate position 9 (clamp).

Fig. 12 Convergence behavior of the best objective function value of the six optimization runs for the Gaussian distributed damage scenario of fishplate positions 1 and 9 using the Gaussian damage distribution function

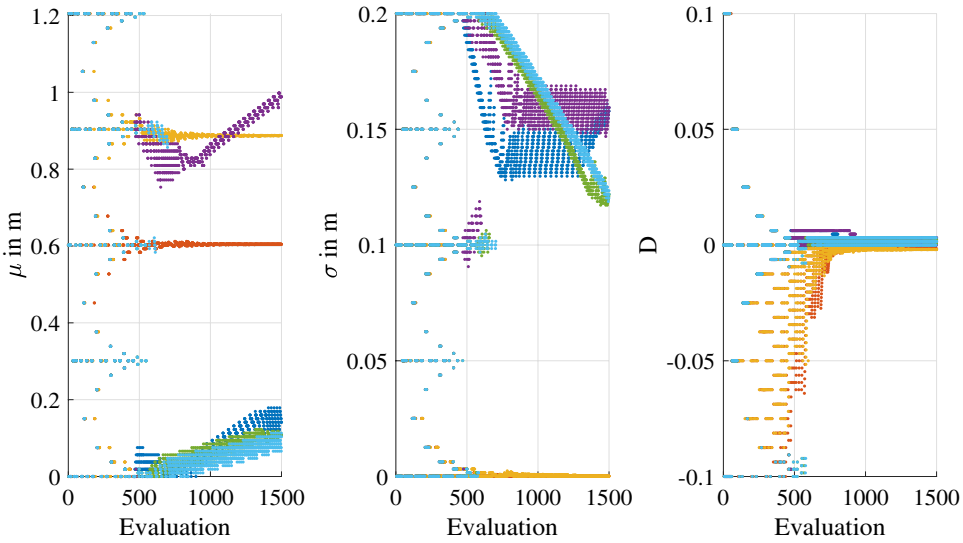

Fig. 13 Convergence behavior of the three design variables of the six optimization runs for the Gaussian distributed damage scenario of fishplate position 1 (tip) using the Gaussian damage distribution function

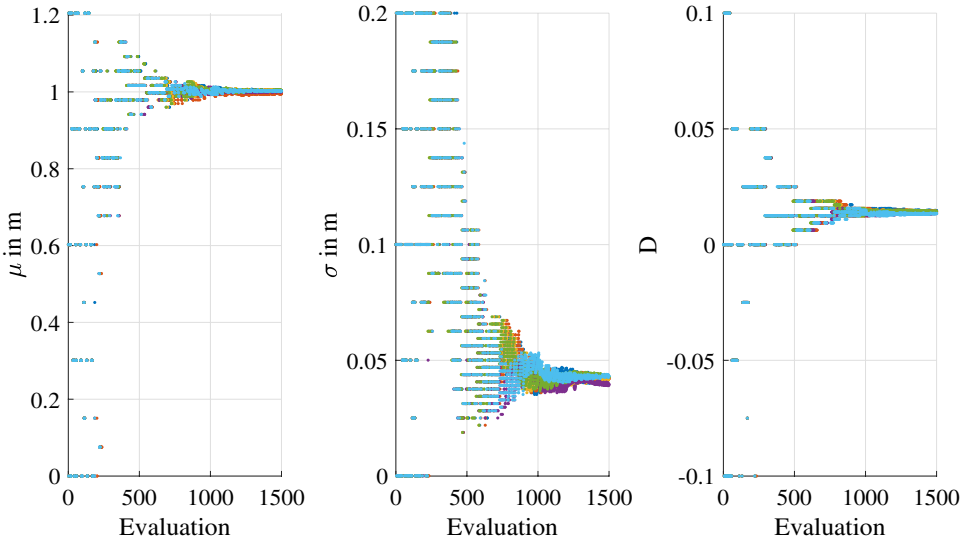

Fig. 14 Convergence behavior of the three design variables of the six optimization runs for the Gaussian distributed damage scenario of fishplate position 9 (clamp) using the Gaussian damage distribution function

behavior of the three design variables for the two damaged states considered.

First of all, a distinct and proper convergence of the optimization algorithm employed is visible, confirming that the maximum number of objective function evaluations is sufficient. Comparing the varying convergence behavior of the design variables and the best objective function value for the two damaged fishplate positions, the influence of the geometric position of the damage along the length of the steel cantilever beam is clearly visible. All six optimization runs regarding fishplate position 9 (clamp) result in almost equivalent design variables and objective function values, presenting a conclusive localization and quantification of this damage scenario. In contrast, the results concerning fishplate position 1 (tip) differ partially significantly from each other. In Fig. 13, the design variable μ, for instance, converges in only three of the six optimization runs towards the correct value of 0.075m while values between 0.6m and 1m are mistakenly found to be optimal in optimization runs 2–4. Additionally, the optimal values found for the design variable σ vary within a range of 0.05 m, representing 25% of the bounded space for this design variable. Only the damage intensity converges to an equivalent value in all six optimization runs. However, this seemingly optimal value is approximately 0, which is incorrect.

This inconclusive convergence behavior concerning the results for fishplate position 1 (tip) indicates a difficult design variable space with multiple local minima. In comparison to the conclusive results regarding fishplate position 9 (clamp), this reveals the difficulty to locate and quantify a damage at a geometric position very close to the tip of the steel cantilever beam compared to the seemingly simple assessment of a damage near the bearing. This conclusion matches the observations and thus the expectations from

Sect. 3, where the modal properties of the different damaged states were studied in detail. A damage positioned near the tip of the steel cantilever beam has no significant influence on the stiffness properties and therefore on the structural behavior, whereas a damage positioned near the bearing has a considerable effect. Thus, even adapting the stiffness of all FEs along the beam length using a comparison of modal properties—as it is employed in the utilized and in most other FE model updating procedures—is naturally limited by the effect a damage has on the (global) stiffness properties and, thus, the global dynamic behavior of the structure considered.

To present the final results, the $9 \cdot 3 \cdot 6$ optimal distributions of the stiffness scaling factor $\boldsymbol{\theta}$ resulting from the respective optimal design variable vectors are displayed in Figs. 15 and 16 for the two damage distribution functions utilized. Thereby, one color is used per damage scenario as depicted in the legend.

Overall, the results of the FE model updating procedure using only eigenfrequencies as the damage sensitive feature demonstrate a conclusive localization of the nine different damage positions (i.e., fishplate positions) and a distinct quantification between the three damage intensities employed. As already mentioned with regard to Figs. 12, 13 and 14, the results for the damaged fishplate position 1 (tip) are especially inconclusive as this is a position where damage has no significant effect on the global dynamic behavior of the steel cantilever beam. Thus, the identification, localization and quantification of a defect at this particular position are very difficult using the proposed or any other FE model updating procedure. Regarding the final results in Figs. 15 and 16 for this position, only the fishplate with the most severe damage (i.e., the uniformly distributed damage) is located correctly, whereas the other two damage scenarios are not found at all. This is the reason why the results for fishplate position 1 at the tip of the steel cantilever beam are not included in the following detailed discussion of the results.

Figure 17 allows for a precise observation of the results of the damage localization (i.e., design variable μ) for fishplate positions 2 to 9. The figure shows the difference between the optimal design variables obtained using the FE model updating procedure and the actual measured (i.e., expected) values, depicted as dotted black lines.

The geometric positions of the discrete damage scenario (blue diamonds) are misidentified in some cases, which is also visible in Figs. 15 and 16. This observation unveils that, naturally, the localization of the discrete damage scenario, having the least damage severity, is more difficult than the identification of the other two more severe damage scenarios. In addition, the localization results using the Gaussian damage distribution function (cf. Fig. 17a) are slightly

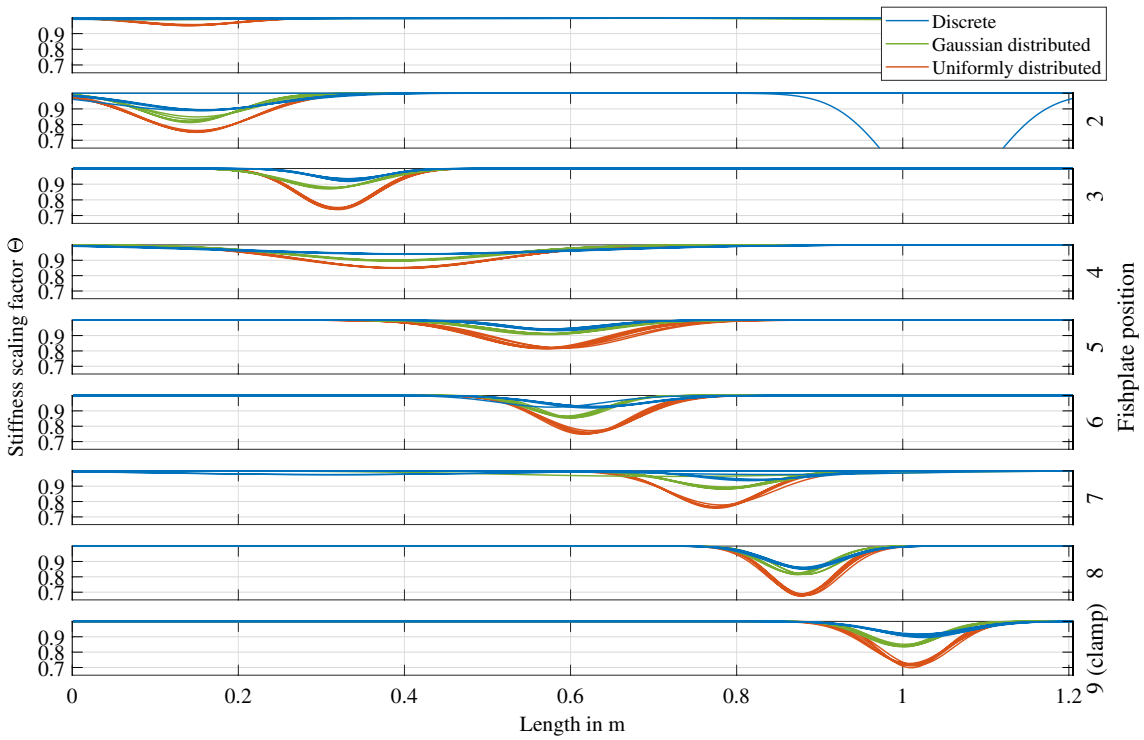

Fig. 15 $9 \cdot 3 \cdot 6$ optimal distributions of the stiffness scaling factor θ for the nine fishplate positions and the three different damage scenarios for the Gaussian damage distribution functions

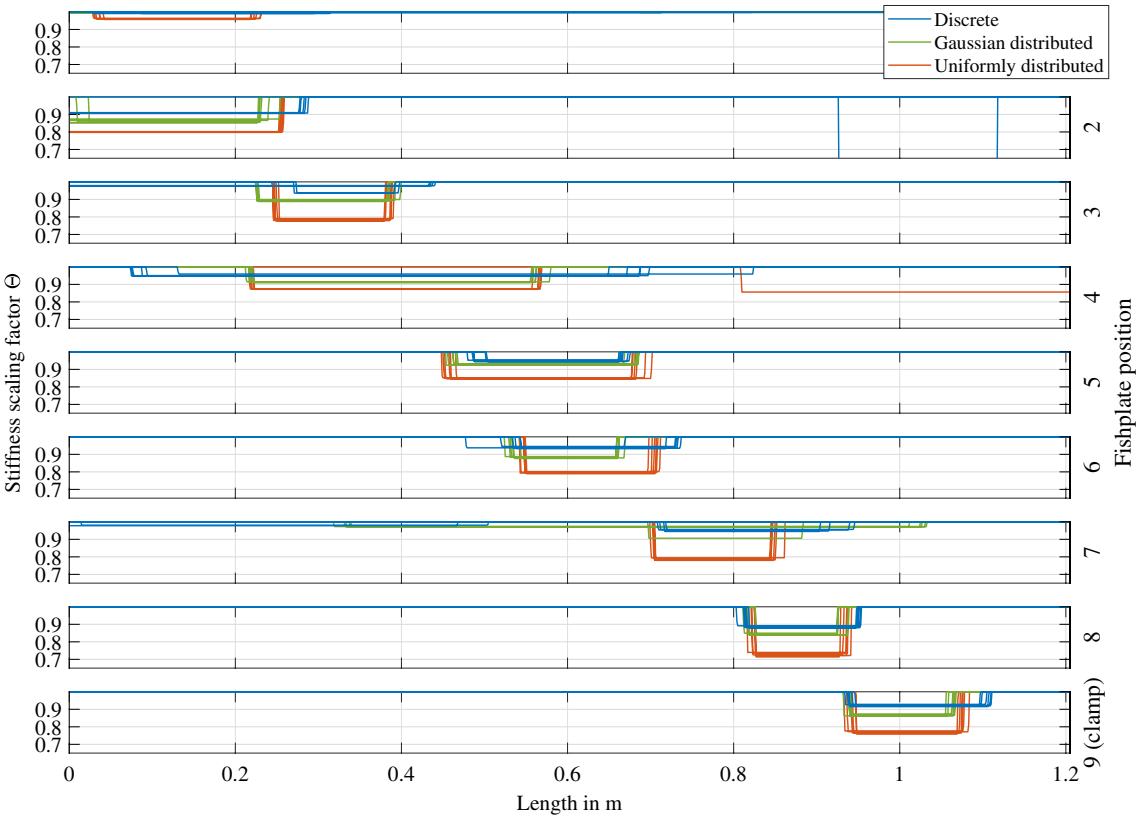

Fig. 16 $9 \cdot 3 \cdot 6$ optimal distributions of the stiffness scaling factor θ for the nine fishplate positions and the three different damage scenarios for the continuous uniform damage distribution functions

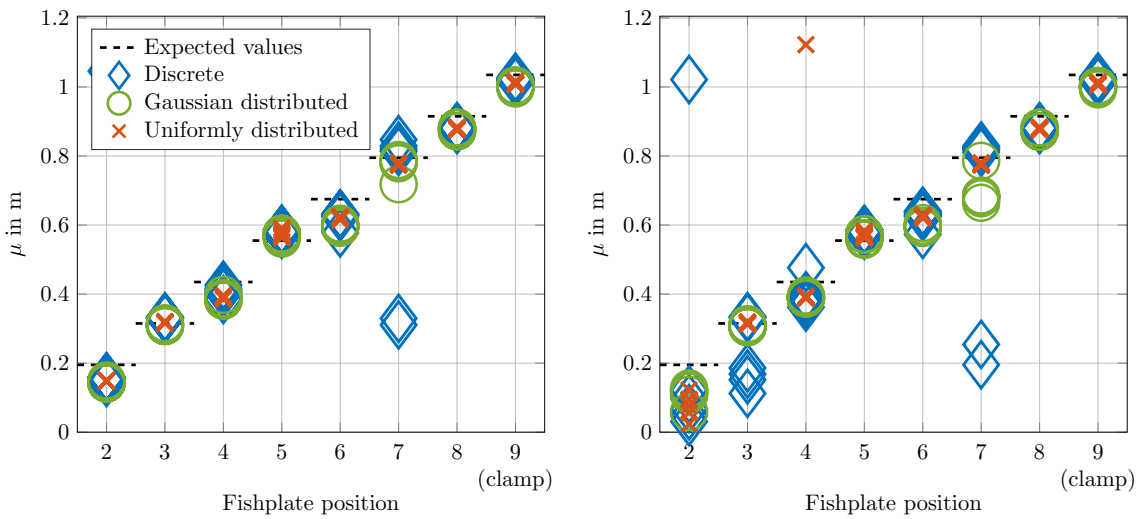

(a) Gaussian. (b) Continuous uniform.

Fig. 17 Comparison of the expected values to the optimal values obtained for the design variable μ for each damage scenario of fishplate positions 2 to 9 using the two damage distribution functions considered

more consistent than the results using the continuous uniform damage distribution function (cf. Fig. 17b). Overall, however, it is evident that the employment of both damage distribution functions yield accurate localization results, in most cases within ±0.05m of the expected geometric position of the different damage scenarios. Thus, a successful localization of all fishplate positions considered is achieved.

The correct values expected for the design variable σ are equal for all fishplate positions per damage scenario as the width of the damage is constant per damage scenario. Thereby, the width of the discrete damage is 0.001m. The width of the Gaussian and the uniformly distributed damage is the same with a value of 0.093m ranging from the first to the last saw cut. Only the damage intensity differs for these two damage scenarios due to the differing lengths of the saw cuts (cf. Fig. 4). Figure 18 displays these expected values, depicted as dotted lines in the color of the respective damage scenario, alongside the optimal values found for the design variable σ obtained by the application of the two damage distribution functions considered. Because of the definition of the design variable σ in the damage distribution functions (cf. Sect. 4.1 and Fig. 10), the optimal values for the design variable are multiplied by two so the expected values are compared to $\pm\sigma$.

Regarding the results for the Gaussian and the uniformly distributed damage scenarios (green circles and red crosses), most of the optimal values obtained vary within a range of 0.06–0.16 m. Only the values obtained for fishplate positions 2 and 4 show more variation, which is again also visible in Figs. 15 and 16. Thus, the width of the two more severe damage scenarios is, in most cases, identified close to the actual width measured to 0.093 m from the first to the last saw cut. This is why the identification of the damage width concerning the Gaussian and the uniformly distributed damage scenario is considered to be successful. It is noticeable that the width of the discrete damage (blue diamonds) is misidentified in all damage positions. As this damage scenario represents a rupture of only 1 mm width in the fishplate specimen (cf. Fig. 4), the results obtained for σ between 0.075 m and 0.2 m regarding this particular damage scenario are clearly incorrect. Again, this reveals the difficulty to identify this least severe damage scenario correctly.

As with the design variable σ, the design variable D is also expected to be equal for all fishplate positions per damage scenario as the intensity of the damage is also constant per damage scenario. For the calculation of the expected values regarding the damage intensity, it is assumed that the alteration of the moment of inertia is proportional to the alteration of the stiffness properties due to the different saw cuts into the fishplate specimens. Hence, the stiffness scaling factor θ_i in Eq. 9 is exchanged with a scaling factor for the moment of inertia of each finite element and the values for D are calculated for the three different damage scenarios, respectively.

The calculated values for D are 0.0005 for the discrete damage scenario, 0.0013 for the Gaussian distributed damage scenario and 0.0024 for the uniformly distributed damage scenario. Compared to the optimal values obtained using the FE model updating procedure, the analytically calculated values are off approximately by a factor of ten. In the case of the Gaussian and uniformly distributed damage scenarios, this is due to the fact that the calculation on the basis of the

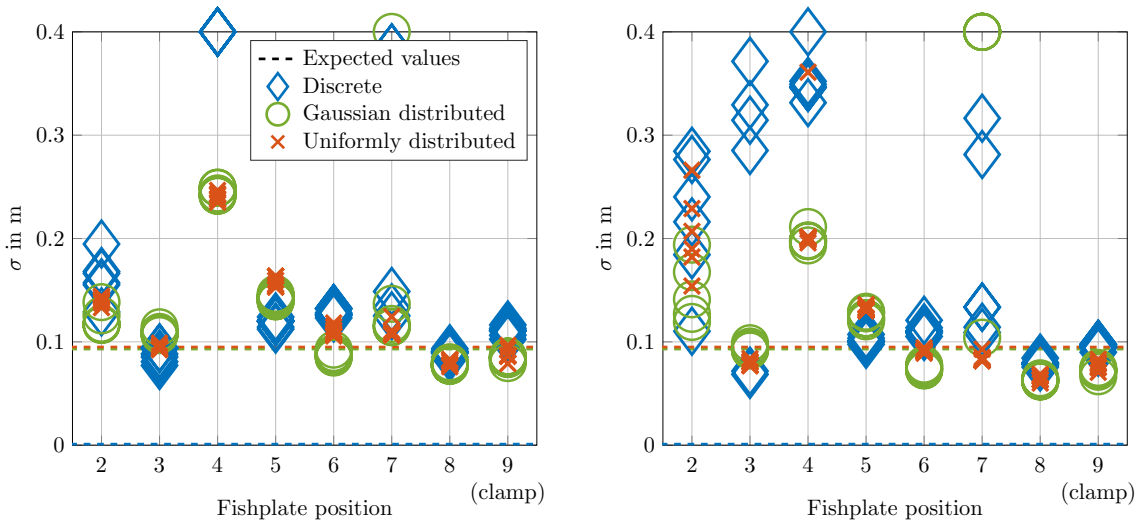

(a) Gaussian.

(b) Continuous uniform.

Fig. 18 Comparison of the expected values to the optimal values obtained for the design variable $\pm\sigma$ for each damage scenario of fishplate positions 2–9 using the two damage distribution functions considered

altered moment of inertia only considers six altered FEs as there are six saw cuts in the respective fishplate specimens (cf. Figure 4). This rather underestimates the damage to the structure as the impact on the stiffness properties is not locally limited to these six FEs. In contrast, the damage distribution functions utilized in the FE model updating process are designed to identify a damaged area. If the moment of inertia of all FEs between the first and last saw cut are scaled according to the induced saw cuts, the values obtained for D are 0.021 for the Gaussian and 0.037 for the uniformly distributed damage scenario. Hence, these values are similar to the optimal values obtained using the model updating procedure. The optimal results for the damage intensity (i.e., design variable D) are displayed in Fig. 19. All results are normalized to the results of the Gaussian distributed damage scenario. This enables a direct comparison of the relative differences in D between the optimization-based solutions and the results for the analytical (moment of inertia-based) calculations. The normalized analytical values for D (0.38 for the discrete, 1 for the Gaussian distributed and 1.85 for the uniformly distributed damage scenario) are depicted as dotted lines in the color of the respective damage scenario.

As expected, the optimal values obtained using the FE model updating procedure are fairly consistent for each damage scenario. In addition, the increasing intensity of the three different damage scenarios is distinctly visible for both damage distribution functions utilized as already discernible in Figs. 15 and 16. The percentage increase of the optimal results is close to the analytically calculated increase in damage severity. For example, the normalized values for D are approximately by a factor of 1.85 higher for the uniformly distributed compared to the Gaussian distributed damage for the analytical as well as the optimization-based results. Only the damage intensity of the discrete damage scenario is slightly overestimated by the model updating procedure. Altogether, the quantification of the different damage severities introduced is considered successful. In particular, it is possible to quantify the relative change in damage intensity which is, for example, relevant when cracks are growing.

6 Conclusions and outlook

With this work, the laboratory experiment of a modular steel cantilever beam with the option to insert different damage scenarios at different positions is presented in detail and the measurement data is made available in open-access form. In addition, a systematic experimental validation of a deterministic FE model updating procedure using four eigenfrequencies as damage sensitive features is demonstrated.

The results presented in Sect. 5 evidently show the successful precise localization of the nine different damage positions within ± 0.05m (i.e., $\pm 4\%$) of the correct geometric positions along the 1.2-m-long beam. In addition, the quantification regarding the width and the intensity of the three different damage scenarios are found accurately. The distinctive results emphasize the advantages of the parameterization chosen for the design variables within the model updating process regarding robustness and applicability. In contrast to many conventional FE model updating procedures, the approach proposed is independent of prior assumptions about the defect location and independent of

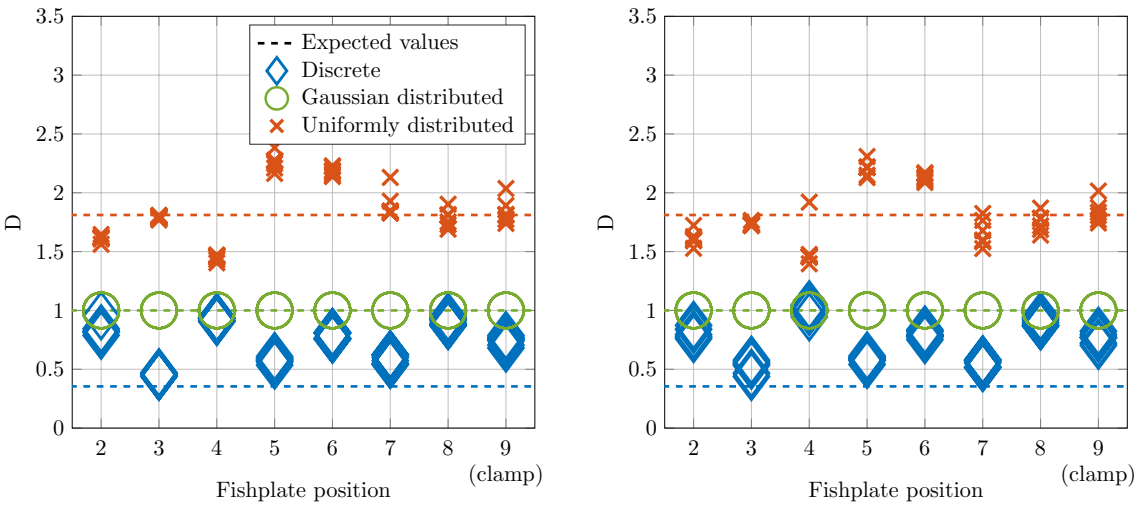

(a) Gaussian.

(b) Continuous uniform.

Fig. 19 Comparison of the normalized analytical values to the optimal values obtained for the normalized design variable D for each damage scenario of fishplate positions 2 to 9 using the two damage distribution functions considered. All values are normalized to the results of the Gaussian distributed damage scenario

the FE mesh resolution while only needing few (in this case three) design variables. The parameterization of a damage distribution function instead of the common mapping of the design variables directly to structural properties ensures a realistic distribution of the stiffness properties of the structure considered. Also, the extension of the model updating procedure lends itself to easily exchange different damage distribution functions and, hence, offers the opportunity to imitate different damage modes. Additionally, the experimentally validated formulation of the objective function using a relative eigenfrequency metric enables the usage of a minimal sensor concept for damage assessment. Furthermore, the demonstration of the experimental validation of the FE model updating approach utilized reveals the applicability of the laboratory experiment presented for the validation of SHM procedures addressing damage assessment. With the experimental setup enabling the opportunity to introduce reversible damage scenarios of differing damage severities at a total of nine different damage positions, a fundamental evaluation and comparison of different SHM methods is possible.

Looking more closely, naturally, some difficulties occurred and some observations are made regarding the outlook of this work. The damage position at the tip of the steel cantilever beam was difficult to localize and quantify correctly as a damage at this position has no significant influence on the stiffness properties and, thus, on the structural behavior of the steel cantilever beam. As a result, this particular damage scenario differs only marginally from the reference state, which results in a difficult design variable space, making it almost impossible for the optimization algorithm applied to find a correct solution. However, this finding represents a difficulty for all damage assessment methods based on modal parameters as they rely on the variation of the global structural behavior. In addition, the results of the discrete (i.e., the least intense) damage scenario show more variance with regard to the correct values than the other two more severe damage scenarios. Especially the width of this damage scenario is clearly overestimated. Further studies will include additional or different damage sensitive features potentially in a second objective function in order to analyze possible improvements enabled by multi-objective optimization.

Another interesting next step is the inclusion of the uncertainty regarding the modal properties. Therefore, the experiment is especially suited since the uncertainties are distinctly quantifiable in the laboratory experiment designed using the long 1-h measurements of the different damage scenarios and the, respectively, following repetitions of the measurements in reference state.

Acknowledgements We greatly acknowledge the financial support of the German Federal Ministry for Economic Affairs and Energy (research project *Multivariates Schadensmonitoring von Rotorblättern*, FKZ 0324157A) and Deutsche Bundesstiftung Umwelt (research project *Gebrauchstauglichkeit und Komfort von dynamisch beanspruchten Holztragwerken im urbanen mehrgeschossigen Hochbau*, AZ 34548/01-25) that enabled this work. In addition, we gratefully acknowledge the financial support of the Deutsche Forschungsgemeinschaft (DFG, German Research Foundation) - SFB-1463-434502799.

Funding Open Access funding enabled and organized by Projekt DEAL.

Data availability statement The measurement data used in this work including a comprehensive documentation are published as an open-access data publication within the Research Data Repository of the Leibniz University Hanover that issues datasets with DOIs: https://doi.org/10.25835/123gy6gm.

References

1. Brownjohn J (2007) Structural health monitoring of civil infrastructure. Philos Trans R Soc A Math Phys Eng Sci 365(1851):589–622. https://doi.org/10.1098/rsta.2006.1925
2. Avci O, Abdeljaber O, Kiranyaz S, Hussein M, Gabbouj M, Inman DJ (2021) A review of vibration-based damage detection in civil structures: from traditional methods to machine learning and deep learning applications. Mech Syst Signal Process 147:107077. https://doi.org/10.1016/j.ymssp.2020.107077
3. Doebling SW, Farrar CR, Prime MB (1998) A summary review of vibration-based damage identification methods. Shock Vib Dig 30:91–105
4. Carden EP, Fanning P (2004) Vibration based condition monitoring: a review. Struct Health Monit 3(4):355–377. https://doi.org/10.1177/1475921704047500
5. Fan W, Qiao P (2011) Vibration-based damage identification methods: a review and comparative study. Struct Health Monit 10(1):83–111. https://doi.org/10.1177/1475921710365419
6. Das S, Saha P, Patro SK (2016) Vibration-based damage detection techniques used for health monitoring of structures: a review. J Civ Struct Health Monit 6(3):477–507. https://doi.org/10.1007/s13349-016-0168-5
7. Worden K, Farrar CR, Manson G, Park G (2007) The fundamental axioms of structural health monitoring. Proc R Soc A Math Phys Eng Sci 463(2082):1639–1664. https://doi.org/10.1098/rspa.2007.1834
8. Rytter A (1993) Vibrational based inspection of civil engineering structures, no. 44 in fracture and dynamics. Department of Building Technology and Structural Engineering, Aalborg University
9. Doebling S, Farrar C, Prime M, Shevitz D (1996) Damage identification and health monitoring of structural and mechanical systems from changes in their vibration characteristics: a literature review,

Tech. Rep. LA–13070-MS, 249299, Los Alamos National Laboratory. https://doi.org/10.2172/249299
10. Sanders D, Kim Y, Stubbs N (1992) Nondestructive evaluation of damage in composite structures using modal parameters. Exp Mech 240–251
11. Abdel Wahab M, De Roeck G, Peeters B (1999) Parameterization of damage in reinforced concrete structures using model updating. J Sound Vib 228(4):717–730. https://doi.org/10.1006/jsvi.1999.2448
12. Ju FD, Mimovich ME (1988) Experimental diagnosis of fracture damage in structures by the modal frequency method. J Vib Acoust 110(4):456–463. https://doi.org/10.1115/1.3269550
13. Manoach E, Warminski J, Kloda L, Teter A (2017) Numerical and experimental studies on vibration based methods for detection of damage in composite beams. Compos Struct 170:26–39. https://doi.org/10.1016/j.compstruct.2017.03.005
14. Schröder K, Gebhardt CG, Rolfes R (2018) A two-step approach to damage localization at supporting structures of offshore wind turbines. Struct Health Monit 17(5):1313–1330. https://doi.org/10.1177/1475921717741083
15. Mottershead JE, Link M, Friswell MI (2011) The sensitivity method in finite element model updating: a tutorial. Mech Syst Signal Process 25(7):2275–2296. https://doi.org/10.1016/j.ymssp.2010.10.012
16. Gorgin R (2020) Damage identification technique based on mode shape analysis of beam structures. Structures 27:2300–2308. https://doi.org/10.1016/j.istruc.2020.08.034
17. Figueiredo E, Flynn E (2009) Three-story building structure to detect nonlinear effects. In: Report SHMTools data description
18. Figueiredo E, Park G, Figueiras J, Farrar C, Worden K (2009) Structural health monitoring algorithm comparisons using standard data sets, Tech. Rep. LA-14393, Los Alamos National Laboratory. https://doi.org/10.2172/961604
19. Johnson EA, Lam HF, Katafygiotis LS, Beck JL (2001) A benchmark problem for structural health monitoring and damage detection. In: Structural control for civil and infrastructure engineering. World Scientific, pp 317–324. https://doi.org/10.1142/9789812811707_0028
20. Dyke SJ, Bernal D, Beck JL, Ventura C (2001) An experimental benchmark problem in structural health monitoring. In: Proceedings of the 3rd international workshop on structural health monitoring, pp 1–10
21. Krämer C, De Smet C, De Roeck G (1999) Z24 bridge damage detection tests. In: Proceedings of the 17th international modal analysis conference, pp 1023–1029
22. Maeck J, De Roeck G (1999) Damage detection on a prestressed concrete bridge and rc beams using dynamic system identification. Key Eng Mater 167–168:320–327. https://doi.org/10.4028/www.scientific.net/KEM.167-168.320
23. Tcherniak D, Larsen GC (2013) Application of oma to an operating wind turbine: now including vibration data from the blades. In: Proceedings of the 5th international operational modal analysis conference, pp 1–12
24. Tcherniak D, Mølgaard LL (2015) Vibration-based shm system: application to wind turbine blades. J Phys Conf Ser 628:012072. https://doi.org/10.1088/1742-6596/628/1/012072
25. Bull T, Ulriksen MD, Tcherniak D (2018) The effect of environmental and operational variabilities on damage detection in wind turbine blades. In: Proceedings of the 9th European workshop on structural health monitoring, pp 1–9
26. Wernitz S, Hofmeister B, Jonscher C, Grießmann T, Rolfes R (2022) A new open-database benchmark structure for vibration-based structural health monitoring. Struct Control Health Monit. https://doi.org/10.13140/RG.2.2.26051.48163
27. Hübler C, Hofmeister B, Wernitz S, Rolfes R (2022) Validierung von daten- und modellbasierten methoden zur schadenslokalisierung. Bautechnik 99(6):433–440. https://doi.org/10.1002/bate.202200015
28. Levinzon F (2015) Piezoelectric accelerometers with integral electronics. Springer International Publishing. https://doi.org/10.1007/978-3-319-08078-9
29. Timoshenko SP (1921) On the correction for shear of the differential equation for transverse vibrations of prismatic bars. Lond Edinb Dublin Philos Mag J Sci 41(245):744–746. https://doi.org/10.1080/14786442108636264
30. Brincker R, Zhang L, Andersen P (2001) Modal identification of output-only systems using frequency domain decomposition. Smart Mater Struct 10(3):441–445. https://doi.org/10.1088/0964-1726/10/3/303
31. Brincker R, Ventura C, Andersen P (2001) Damping estimation by frequency domain decomposition. In: Proceedings of the 19th international modal analysis conference, pp 698–703
32. Brincker R, Ventura CE (2015) Introduction to operational modal analysis. Wiley, Chichester. https://doi.org/10.1002/9781118535141
33. Allemang RJ, Brown DL (1982) A correlation coefficient for modal vector analysis. In: Proceedings of the 1st international modal analysis conference, vol 1, pp 110–116
34. Mottershead JE, Friswell MI (1993) Model updating in structural dynamics: a survey. Journal of Sound and Vibration 167(2):347–375. https://doi.org/10.1006/jsvi.1993.1340
35. Simoen E, De Roeck G, Lombaert G (2015) Dealing with uncertainty in model updating for damage assessment: a review. Mech Syst Signal Process 56–57:123–149. https://doi.org/10.1016/j.ymssp.2014.11.001
36. Friswell MI, Mottershead JE (1995) Finite element model updating in structural dynamics, vol. 38 of solid mechanics and its applications. Springer Netherlands. https://doi.org/10.1007/978-94-015-8508-8
37. Friswell MI (2007) Damage identification using inverse methods. Philos Trans R Soc A Math Phys Eng Sci 365(1851):393–410. https://doi.org/10.1098/rsta.2006.1930
38. Link M (1999) Updating of analytical models—review of numerical procedures and application aspects. In: Proceedings of the structural dynamics forum. Research Studies Press, Baldock, pp 193–223
39. Zhang Z, Luo Y (2017) Restoring method for missing data of spatial structural stress monitoring based on correlation. Mech Syst Signal Process 91:266–277. https://doi.org/10.1016/j.ymssp.2017.01.018
40. Reynders E (2012) System identification methods for (operational) modal analysis: review and comparison. Arch Comput Methods Eng 19(1):51–124. https://doi.org/10.1007/s11831-012-9069-x
41. Beck JL, Katafygiotis LS (1998) Updating models and their uncertainties. I: Bayesian statistical framework. J Eng Mech 124(4):455–461. https://doi.org/10.1061/(ASCE)0733-9399(1998)124:4(455)
42. Katafygiotis LS, Yuen K-V (2001) Bayesian spectral density approach for modal updating using ambient data. Earthq Eng Struct Dyn 30(8):1103–1123. https://doi.org/10.1002/eqe.53
43. Hizal C, Turan G (2020) A two-stage Bayesian algorithm for finite element model updating by using ambient response data from multiple measurement setups. J Sound Vib 469:115139. https://doi.org/10.1016/j.jsv.2019.115139
44. Liu P, Huang S, Song M, Yang W (2021) Bayesian model updating of a twin-tower masonry structure through subset simulation optimization using ambient vibration data. J Civ Struct Health Monit 11(1):129–148. https://doi.org/10.1007/s13349-020-00443-y
45. Savoia M (2002) Structural reliability analysis through fuzzy number approach, with application to stability. Comput Struct

80(12):1087–1102. https://doi.org/10.1016/S0045-7949(02)00068-8
46. Haag T, Herrmann J, Hanss M (2010) Identification procedure for epistemic uncertainties using inverse fuzzy arithmetic. Mech Syst Signal Process 24(7):2021–2034. https://doi.org/10.1016/j.ymssp.2010.05.010
47. Haag T, Carvajal González S, Hanss M (2012) Model validation and selection based on inverse fuzzy arithmetic. Mech Syst Signal Process 32:116–134. https://doi.org/10.1016/j.ymssp.2011.09.028
48. Levin R, Lieven N (1998) Dynamic finite element model updating using simulated annealing and genetic algorithms. Mech Syst Signal Process 12(1):91–120. https://doi.org/10.1006/mssp.1996.0136
49. Teughels A, Maeck J, De Roeck G (2002) Damage assessment by FE model updating using damage functions. Comput Struct 80(25):1869–1879. https://doi.org/10.1016/S0045-7949(02)00217-1
50. García-Palencia AJ, Santini-Bell E (2014) Structural model updating using dynamic data. J Civ Struct Health Monit 4(3):177–194. https://doi.org/10.1007/s13349-014-0073-8
51. Kim G-H, Park Y-S (2004) An improved updating parameter selection method and finite element model update using multiobjective optimisation technique. Mech Syst Signal Process 18(1):59–78. https://doi.org/10.1016/S0888-3270(03)00042-6
52. García-Palencia AJ, Santini-Bell E (2013) A two-step model updating algorithm for parameter identification of linear elastic damped structures. Comput Aided Civ Infrastruct Eng 28:509–521. https://doi.org/10.1111/mice.12012
53. Bruns M, Hofmeister B, Hübler C, Rolfes R (2019) Damage localization via model updating using a damage distribution function. In: Structural health monitoring 2019. DEStech Publications Inc, pp 909–917https://doi.org/10.12783/shm2019/32202
54. Bruns M, Hofmeister B, Grießmann T, Rolfes R (2019) Comparative study of parameterizations for damage localization with finite element model updating. In: Proceedings of the 29th European safety and reliability conference. Res Publ Serv. https://doi.org/10.3850/978-981-11-2724-3_0713-cd
55. Teughels A, De Roeck G, Suykens JA (2003) Global optimization by coupled local minimizers and its application to FE model updating. Comput Struct 81(24–25):2337–2351. https://doi.org/10.1016/S0045-7949(03)00313-4
56. Schommer S, Nguyen VH, Maas S, Zürbes A (2017) Model updating for structural health monitoring using static and dynamic measurements. Procedia Eng 199:2146–2153. https://doi.org/10.1016/j.proeng.2017.09.156
57. Schommer S, Dakhili K, Nguyen VH, Kebig T, Zürbes A, Maas S (2022) A gaussian damage function combined with sliced finite-element meshing for damage detection. J Civ Struct Health Monit 12:1493–1508. https://doi.org/10.1007/s13349-022-00602-3
58. Teughels A, De Roeck G (2003) Damage Assessment of the Z24 Bridge by FE Model Updating. Key Eng Mater 245–246:19–26. https://doi.org/10.4028/www.scientific.net/KEM.245-246.19
59. Coello Coello CA (2002) Theoretical and numerical constraint-handling techniques used with evolutionary algorithms: a survey of the state of the art. Comput Methods Appl Mech Eng 191(11):1245–1287. https://doi.org/10.1016/S0045-7825(01)00323-1
60. Berger R, Bruns M, Ehrmann A, Haldar A, Häfele J, Hofmeister B, Hübler C, Rolfes R (2021) Engio-object-oriented framework for engineering optimization. Adv Eng Softw 153:102959. https://doi.org/10.1016/j.advengsoft.2020.102959
61. Hofmeister B, Bruns M, Rolfes R (2019) Finite element model updating using deterministic optimisation: a global pattern search approach. Eng Struct 195:373–381. https://doi.org/10.1016/j.engstruct.2019.05.047